

Conduction failure in axonal signal propagation: Effects of I_h in a Hodgkin-Huxley cable model

Rong Hu(胡榕) and Yong Xie(谢勇)

Citation: Chin. Phys. B, 2026, 35 (**6**): 068706. DOI: 10.1088/1674-1056/ae5c7a
http://cpb.iphy.ac.cn; http://iopscience.iop.org/cpb

What follows is a list of articles you may be interested in

Spatial heterogeneity of axon induces complex dynamics of enhanced conduction failure rate and irregular pattern of action potentials

Xinjing Zhang(张新景), Yuye Li(李玉叶), Linan Guan(关利南), and Huaguang Gu(古华光)
Chin. Phys. B, 2026, 35 (**6**): 068704. DOI: 10.1088/1674-1056/ae311c

Analysis and image encryption of memristive chaotic system with coexistence bubble

Da Qiu(邱达), Bo Zhang(张博), Tingting Zhang(张婷婷), Song Liu(刘嵩), and Peiyu He(何培宇)
Chin. Phys. B, 2025, 34 (**4**): 040203. DOI: 10.1088/1674-1056/adbee5

Prediction of collapse process and tipping points for mutualistic and competitive networks with *k*-core method

Dongli Duan(段东立), Feifei Bi(毕菲菲), Sifan Li(李思凡), Chengxing Wu(吴成星), Changchun Lv(吕长春), and Zhiqiang Cai(蔡志强)
Chin. Phys. B, 2024, 33 (**5**): 050201. DOI: 10.1088/1674-1056/ad3341

Spatial patterns of the Brusselator model with asymmetric Lévy diffusion

Hongwei Yin(尹洪位), Shangtao Yang(杨尚涛), Xiaoqing Wen(文小庆), Haohua Wang(王浩华), and Shufen Yang(杨淑芬)
Chin. Phys. B, 2024, 33 (**11**): 110202. DOI: 10.1088/1674-1056/ad74e5

On fractional discrete financial system: Bifurcation, chaos, and control

Louiza Diabi, Adel Ouannas, Amel Hioual, Shaher Momani, and Abderrahmane Abbes
Chin. Phys. B, 2024, 33 (**10**): 100201. DOI: 10.1088/1674-1056/ad5d96

SPECIAL TOPIC — Biophysical circuits: Modeling & applications in neuroscience

Conduction failure in axonal signal propagation: Effects of I_h in a Hodgkin–Huxley cable model

Rong Hu(胡榕) and Yong Xie(谢勇)[†]

State Key Laboratory for Strength and Vibration of Mechanical Structures, Shaanxi Engineering Research Center of Nondestructive Testing and Structural Integrity Evaluation, School of Aerospace Engineering, Xi'an Jiaotong University, Xi'an 710049, *China*

(Received 6 March 2026; revised manuscript received 4 April 2026; accepted manuscript online 8 April 2026)

Axonal conduction failure, characterized by spike loss during propagation, represents a fundamental nonlinear phenomenon underlying unreliable signal conduction in excitable media, but its dynamical origins remain unclear. Here, we develop a Hodgkin–Huxley cable model to investigate conduction failure during axonal propagation, incorporating the hyperpolarization-activated cyclic nucleotide-gated (I_h) current. By varying the I_h conductance g_h, diffusion coefficient D, stimulation period T_s, and temperature T, we quantify conduction reliability using conduction rate and conduction velocity. Increasing g_h elevates the resting potential and expands the parameter region supporting faithful conduction. Conduction rate maps in the (T_s, D) plane reveal that reliable conduction requires sufficient axial diffusion and appropriate input timing. Conduction velocity increases monotonically with D but shows nontrivial dependence on T_s and g_h. Temperature reshapes axonal conduction dynamics by suppressing spike initiation at low T and inducing spike multiplication at high T. Bifurcation analysis links these effects to T- and g_h-dependent shifts of saddle-node and Hopf bifurcation boundaries.

Keywords: Hodgkin–Huxley model, hyperpolarization-activated cation current, conduction failure, conduction velocity

PACS: 87.19.lq, 02.30.Oz, 05.45.–a

DOI: 10.1088/1674-1056/ae5c7a **CSTR:** 32038.14.CPB.ae5c7a

1. Introduction

In spatially extended neuronal systems such as axons, the reliable propagation of action potentials (or "spikes") constitutes the physical basis of neural information transmission.[1–3] Within the framework of excitable media, an action potential behaves as a traveling nonlinear wave sustained by the balance between local membrane excitability and axial current flow governed by cable diffusion. However, spike propagation is not always guaranteed. Action potentials may attenuate or disappear during conduction, leading to conduction failure manifested as spike loss, which directly limits the fidelity of neural signaling.[4–6] Understanding the mechanisms that determine whether propagation succeeds or fails, therefore, remains a fundamental problem in neurodynamics and nonlinear wave theory. The classical Hodgkin–Huxley (HH) model provides the standard biophysical description of membrane excitability.[7] When extended in space through the cable formulation, it enables the investigation of action potential propagation along axons by combining ionic membrane dynamics with axial diffusion currents.[2] Previous studies based on the HH cable framework have identified several mechanisms underlying conduction failure during axonal propagation. In particular, spike conduction may fail when axial current flow is insufficient to depolarize downstream membrane regions to the firing threshold or when stimulation frequencies exceed the recovery capability of ionic channels. Experimental and theoretical investigations have demonstrated that refractory dynamics, activity-dependent excitability regulation, and membrane biophysical properties play essential roles in determining propagation reliability.[8–13] Recent studies have further highlighted the importance of channel cooperation and signal transmission regulation in neuronal information processing, including sodium-channel cooperative activation mechanisms and artificial synaptic systems capable of modulating signal conduction speed.[14,15]

Despite these advances, most existing studies primarily focus on intrinsic channel kinetics or passive cable properties, while the influence of modulatory ionic currents that continuously reshape membrane excitability during spatial propagation remains less understood.

One such current is the hyperpolarization-activated cation current (I_h), which is widely known to regulate resting membrane potential, neuronal responsiveness, and rhythmic activity.[16–20] Experimental and theoretical studies have shown that I_h can modify excitability and alter action potential conduction velocity through spike-triggered activation of a depolarizing inward current during membrane hyperpolarization.[21,22] Despite these advances, its influence on the stability of long-distance spike propagation in spatially extended axons remains unclear. In particular, it is not known whether I_h consistently promotes reliable propagation

[†]Corresponding author. E-mail: yxie@mail.xjtu.edu.cn

© 2026 Chinese Physical Society and IOP Publishing Ltd. All rights, including for text and data mining, AI training, and similar technologies, are reserved.

or whether, under certain dynamical conditions, it may also promote conduction failure manifested as spike loss.

In this work, conduction failure is defined as the loss of reliable spike-by-spike conduction during axonal propagation. Specifically, conduction failure occurs whenever one or more action potentials generated at the stimulation site fail to reach the distal recording location. Accordingly, spike loss is regarded as the observable manifestation of conduction failure rather than an independent phenomenon. This unified definition is adopted throughout the paper to ensure consistency between numerical observations and dynamical interpretation. Based on this definition, we investigate conduction failure using a HH cable model incorporating the hyperpolarization-activated current. I_h is incorporated as an additional active membrane current that modulates intrinsic excitability within the established cable framework. By systematically varying the maximal I_h conductance g_h, the diffusion coefficient D, and the stimulation period T_s, we examine how intrinsic membrane regulation interacts with spatial propagation dynamics. Conduction reliability is quantified using the conduction rate (R) and conduction velocity (CV). Mapping R in the (T_s, D) parameter plane reveals how I_h reshapes the transition boundary between faithful conduction and conduction failure. Temperature is further introduced as a global kinetic scaling factor to explore how excitability modulation influences propagation stability. Finally, bifurcation analysis of the underlying HH dynamics links macroscopic propagation behavior with changes in dynamical stability.

The structure of this paper is as follows. In Section 2, we introduce the HH cable model and the formulation of the I_h current together with definitions of R and CV. Section 3 presents the numerical results, where we first examine the individual and combined effects of g_h, D, and T_s on axonal conduction (Section 3.1). The global dependence of conduction reliability is then summarized by contour maps of R on the (T_s, D) plane (Subsection 3.2). Next, the multi-parameter modulation of conduction velocity is analyzed (Subsection 3.3), followed by an investigation of temperature effects and their underlying bifurcation mechanisms (Subsection 3.4). Finally, Section 4 summarizes the main conclusions and discusses implications for axonal signal conduction and nonlinear wave propagation in excitable systems.

2. Hodgkin–Huxley cable model and conduction calculations

To investigate the spatial propagation of action potentials, we employ the classical HH cable model describing an unmyelinated axon as a continuous cylindrical fiber. In this framework, membrane excitability governed by ionic channel dynamics is combined with axial current diffusion along the fiber, allowing action potentials to propagate as nonlinear traveling waves. The governing equation for the membrane potential $V(x,t)$ along the axon is

$$\frac{\partial V}{\partial t} = \frac{1}{C_{\rm M}}\Big[-g_{\rm Na}m^3h(V-E_{\rm Na})-g_{\rm K}n^4(V-E_{\rm K}) -g_{\rm L}(V-E_{\rm L})-g_hH(V-E_h)+D\frac{\partial^2V}{\partial x^2}+I_{\rm app}\Big], \quad (1)$$

where V denotes the membrane potential and D represents the axial diffusion coefficient arising from classical cable theory. The diffusion term accounts for longitudinal current flow responsible for signal propagation along the axon. The gating variables m, h, n, and H describe sodium channel activation, sodium channel inactivation, potassium channel activation, and the open probability of the hyperpolarization-activated cation current, respectively. Each gating variable follows first-order dynamics of the form

$$\begin{aligned}
\frac{{\rm d}m}{{\rm d}t} &= \alpha_m(V)(1-m)-\beta_m(V)m,\\
\frac{{\rm d}h}{{\rm d}t} &= \alpha_h(V)(1-h)-\beta_h(V)h,\\
\frac{{\rm d}n}{{\rm d}t} &= \alpha_n(V)(1-n)-\beta_n(V)n,\\
\frac{{\rm d}H}{{\rm d}t} &= \frac{H_\infty(V)-H}{\tau_H(V)}.
\end{aligned} \quad (2)$$

α_m, β_m, α_h, β_h, α_n, β_n, H_∞, τ_H are functions of V given by

$$\begin{aligned}
&\alpha_m = \frac{0.1(V+45)}{1-{\rm e}^{-(V+45)/10}},\ \ \beta_m = 4{\rm e}^{-(V+70)/18},\\
&\alpha_h = 0.07{\rm e}^{-(V+70)/20},\ \ \beta_h = \frac{1}{1+{\rm e}^{-(V+40)/10}},\\
&\alpha_n = \frac{0.01(V+60)}{1-{\rm e}^{-(V+60)/10}},\ \ \beta_n = \frac{1}{8}{\rm e}^{-(V+70)/80},\\
&H_\infty = \frac{1}{1+{\rm e}^{(V+85)/7.3}},\\
&\tau_H = 2000\left[\frac{-7.4(V+60)}{{\rm e}^{-(V+60)/0.8}-1}+65{\rm e}^{-(V+56)/23}\right]^{-1}.
\end{aligned} \quad (3)$$

The ionic currents consist of the standard HH sodium, potassium, and leakage currents together with the hyperpolarization-activated current I_h. The maximal conductance g_h is treated as a control parameter that modulates intrinsic membrane excitability within the HH cable framework. Model parameters are chosen as follows: $C_{\rm M} = 1$ μF/cm^2 is the membrane capacitance, and $I_{\rm app} = -3$ μA/cm^2 represents the externally applied current. The equilibrium potentials are $E_{\rm Na} = 50$ mV, $E_{\rm K} = -77$ mV, $E_{\rm L} = -59$ mV, and $E_h = -30$ mV, for the sodium, potassium, leakage, and hyperpolarization-activated cation currents, respectively. The maximal conductances are $g_{\rm Na} = 120$ mS/cm^2, $g_{\rm K} = 36$ mS/cm^2, $g_{\rm L} = 0.3$ mS/cm^2, and, under normal physiological conditions, $g_h = 2.54$ mS/cm^2.[23] Axons are modeled as finite segments with zero longitudinal current at both ends.

The spatial variable x specifies the position along the axon; throughout the study, the axon is aligned with the x-axis, has a total length of 10 cm, and remains in the resting state in the absence of external stimulation. Periodic square current pulses of amplitude 40 μA/cm^2 and duration 2 ms are applied to the axon from 0 cm to 0.2 cm to evoke action potentials. T_s, D, and g_h are chosen as the control parameters to investigate conduction behaviors along the axon. The axial diffusion coefficient D originates from classical cable theory and can be expressed as $D = a/(2R_i)$, where a is the axonal radius and R_i is the axoplasmic resistivity. Using physiological values for unmyelinated axons ($a \approx 0.5$ μm, $R_i \approx 150$ Ω·cm), the resulting diffusion coefficient is on the order of 10^{-4} cm^2/ms, consistent with the parameter range adopted in this study. Propagation reliability is quantified by the conduction rate $R = N_2/N_1$, where N_1 and N_2 represent the number of action potentials generated at the stimulation site and at the axon terminal, respectively. Faithful conduction corresponds to $R = 1$, meaning that every initiated spike successfully propagates along the axon. Conduction failure is identified whenever $R < 1$, indicating that one or more spikes disappear during spatial propagation. The conduction velocity of unmyelinated fibers has been studied previously.[24] In the simulations, CV is estimated from the propagation delay of action potentials along the axon from one end to the other. Specifically, membrane voltage waveforms are recorded at two positions: the end of the stimulation region (0.2 cm) and the distal end of the axon (10 cm). The time difference between the corresponding spike peaks is measured, and CV is calculated as $CV = \Delta x/(T_2 - T_1)$, where $\Delta x = 9.8$ cm is the propagation distance, and T_1 and T_2 are the times of spike generation at 0.2 cm and 10 cm, respectively. The equations of the HH cable model are solved using the fourth-order Runge–Kutta method. Bifurcations are analyzed with the toolbox XPPAUT.[25]

3. Numerical simulation results and analysis

3.1. Effects of g_h, diffusion coefficient (D), and stimulation period (T_s) on conduction stability

To characterize the spatial propagation of stimulation along the axon, we consider the membrane potentials at $x = 0.2$ cm near the stimulation site and at the axon terminal ($x = 10$ cm), denoted by V_1 and V_2, respectively. The comparison between V_1 and V_2 allows a direct assessment of whether action potentials initiated near the stimulus can be faithfully transmitted to the distal end of the axon. To illustrate the role of I_h in axonal spike propagation, we first consider a baseline comparison in which all parameters are fixed except g_h. Fig. 1 illustrates the conduction behavior of action potentials along the axon for $g_h = 2.54$ mS/cm^2 and $g_h = 0$ mS/cm^2, under fixed diffusion strength ($D = 0.0003$ cm^2/ms) and stimulation period ($T_s = 15$ ms). For $g_h = 2.54$ mS/cm^2, Fig. 1(a) shows the membrane potential at two representative locations along the axon: V_1 close to the stimulation region and V_2 at the axon terminal. Action potentials initiated near the stimulation site propagate successfully to the distal end of the axon ($R = 1$), indicating faithful conduction. To further examine the underlying ionic mechanisms, Fig. 1(b) presents the diffusion current (I_D) and I_h recorded at the axon terminal. Notably, the number of peaks in both I_D and I_h is identical to the number of action potential peaks observed in V_2, revealing a one-to-one correspondence between ionic current dynamics and successful spike propagation. The corresponding spatiotemporal diagram of membrane potential is shown in Fig. 1(c), where action potentials propagate continuously along the axon without interruption. When $g_h = 0$ mS/cm^2, the membrane potential traces in Fig. 1(d) indicate incomplete propagation ($R = 0.7143$), with only a subset of action potentials reaching the axon terminal. Consistently, Fig. 1(e) shows reduced and intermittent responses in both I_D and I_h at $x = 10$ cm, and the spatiotemporal diagram in Fig. 1(f) clearly exhibits conduction failure along the axon. These results indicate that the presence of I_h significantly enhances spike propagation and reduces conduction failure. The impact of I_h on axonal conduction under $D = 0.0002$ cm^2/ms and $T_s = 12$ ms was also analyzed. When $g_h = 2.54$ mS/cm^2, five of eight stimulus-evoked spikes successfully propagate from the stimulation site to the axon terminal, yielding $R = 0.625$. In contrast, when $g_h = 0$ mS/cm^2, only half of the initiated action potentials reach the axon terminal, corresponding to $R = 0.5$. This confirms that the conduction behaviors observed in Fig. 1 are directly related to the modulation of I_h.

As shown in Fig. 1(d), when the hyperpolarization-activated cation current is absent ($g_h = 0$ mS/cm^2), action potential propagation becomes unreliable under relatively weak diffusion, resulting in incomplete conduction and a reduced conduction rate. In these cases, spike initiation near the stimulation site does not guarantee successful propagation to the axon terminal. To examine whether conduction failure under $g_h = 0$ mS/cm^2 can be mitigated by strengthening I_D, the diffusion coefficient is increased to 0.0005 cm^2/ms while keeping the stimulation period fixed at $T_s = 15$ ms. The resulting membrane potential traces and spatiotemporal diagram are shown in Fig. 2. As illustrated in Fig. 2(a), seven action potentials are generated near the stimulation site (V_1), and corresponding action potentials are also observed at the axon terminal (V_2), indicating successful propagation. The spatiotemporal diagram in Fig. 2(b) further confirms continuous and uninterrupted conduction along the axon. Under these conditions, the conduction rate reaches $R = 1$, demonstrating that enhanced diffusion coupling can compensate for the absence of I_h and restore faithful conduction. This result highlights the interplay between intrinsic ionic mechanisms and spatial diffusion in determining axonal conduction reliability. Compared with the case of reduced diffusion, the restoration of faithful conduc-

tion at larger D indicates that I_h effectively lowers the diffusion threshold required for stable spike propagation. It should be noted that when the diffusion coefficient is sufficiently small, action potential propagation fails regardless of the presence of I_h. For example, for $g_h = 2.54$ mS/cm^2, $D = 0.0001$ cm^2/ms, and $T_s = 15$ ms, no action potentials can be transmitted to the axon terminal, resulting in $R = 0$. This behavior is expected, as extremely weak diffusion effectively suppresses spatial coupling between neighboring segments, preventing the formation of propagating spikes.

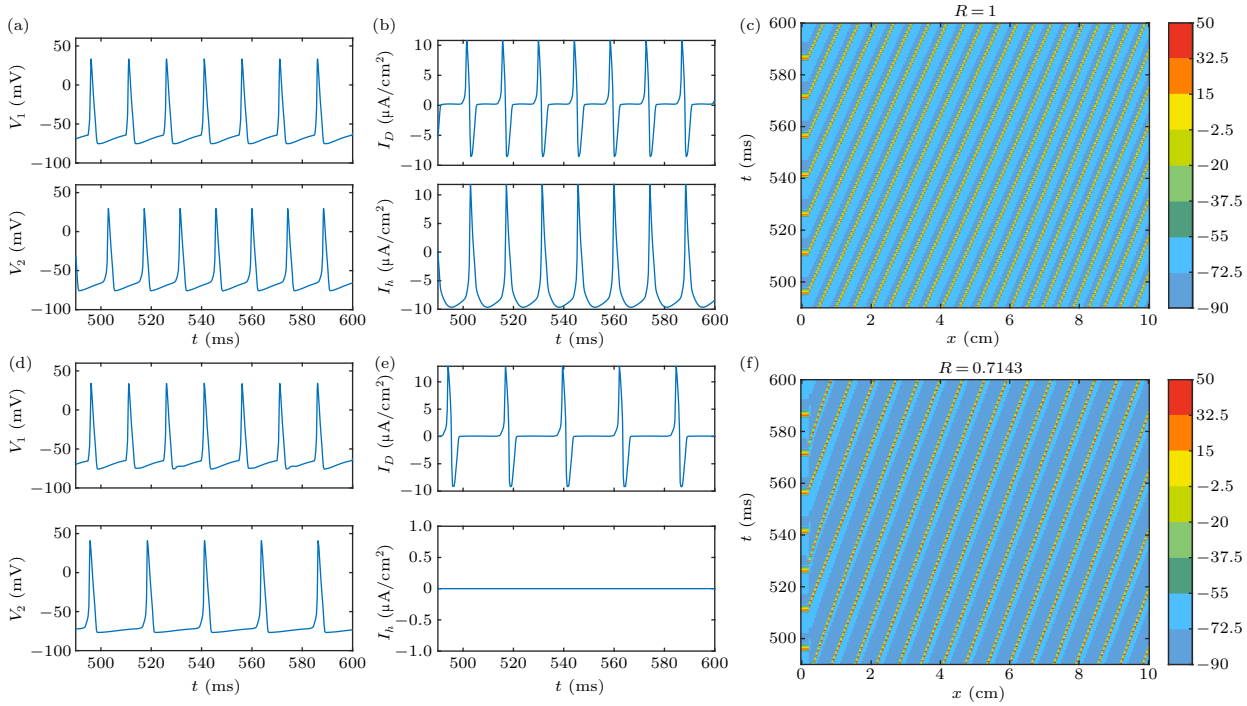


Fig. 1. Spatial propagation of action potentials in the HH cable model for $D = 0.0003$ cm^2/ms and $T_s = 15$ ms. (a) Membrane potential time series at $x = 0.2$ cm (V_1) and $x = 10$ cm (V_2) for $g_h = 2.54$ mS/cm^2. (b) Diffusion current I_D and hyperpolarization-activated current I_h at the axon terminal ($x = 10$ cm) for $g_h = 2.54$ mS/cm^2. (c) Spatiotemporal diagram of action potential propagation along the axon for $g_h = 2.54$ mS/cm^2. (d)–(f) Same as (a)–(c), but for $g_h = 0$ mS/cm^2. The horizontal axis represents the spatial position along the axon, and the vertical axis represents time. Color indicates the membrane potential. Faithful propagation occurs when I_h is present ($R = 1$), whereas intermittent spike loss is observed in the absence of I_h ($R = 0.7143$).

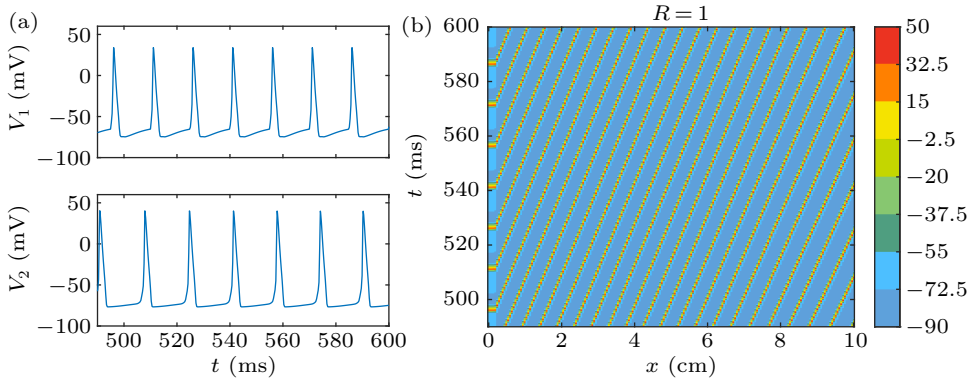


Fig. 2. Restoration of faithful conduction by increasing diffusion strength in the absence of I_h. (a) Membrane potential time series at $x = 0.2$ cm (V_1) and at the axon terminal $x = 10$ cm (V_2) for $g_h = 0$ mS/cm^2, $D = 0.0005$ cm^2/ms, and $T_s = 15$ ms. (b) Corresponding spatiotemporal diagram of membrane potential along the axon, showing continuous propagation and faithful conduction ($R = 1$).

To further clarify the role of the stimulation protocol in axonal conduction reliability, Fig. 3 illustrates how variations in T_s alone can markedly alter conduction behavior, even when intrinsic axonal parameters remain unchanged. When $D = 0.0002$ cm^2/ms, $T_s = 12$ ms, and $g_h = 2.54$ mS/cm^2, this corresponds to $R = 0.625$. In Fig. 3(a), the stimulation period is increased to $T_s = 15$ ms, under which R increases to 1, transitioning from conduction failure to faithful conduction. The corresponding spatiotemporal diagram shows that each action potential propagates sequentially and reaches the axon terminal without loss, indicating faithful conduction. This result highlights the stabilizing effect of a longer stimulation period. In contrast, Fig. 3(b) demonstrates that reducing the stimulation period can exacerbate conduction failure. For $g_h = 0$ mS/cm^2, $D = 0.0003$ cm^2/ms, and $T_s = 10$ ms, the conduction rate decreases to $R = 0.5$, accompanied by pro-

nounced spike loss in the spatiotemporal pattern. Compared with Fig. 1(d), where $T_s = 15$ ms yields a higher conduction rate ($R = 0.7143$), this result confirms that higher stimulation frequency increases the vulnerability of axonal conduction to failure. Together, Fig. 3 demonstrates that conduction failure is not only governed by ion channel expression and diffusion coupling, but is also strongly modulated by the temporal structure of external stimulation. An unfavorable stimulation period can destabilize spike propagation and promote conduction failure, even when other parameters are unchanged.

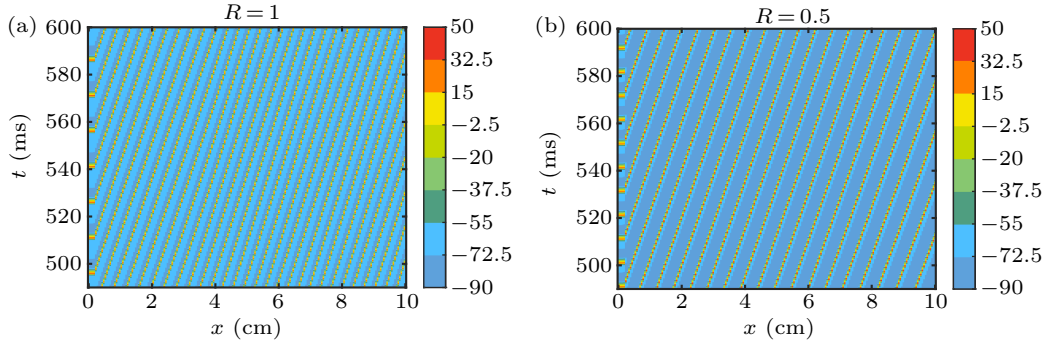


Fig. 3. Influence of the stimulation period T_s on conduction reliability. (a) Faithful propagation for $g_h = 2.54$ mS/cm^2, $D = 0.0002$ cm^2/ms, and $T_s = 15$ ms, with $R = 1$. (b) Conduction failure for $g_h = 0$ mS/cm^2, $D = 0.0003$ cm^2/ms, and $T_s = 10$ ms, where the conduction rate decreases to $R = 0.5$. Varying T_s alone is sufficient to switch between faithful conduction and conduction failure.

In the preceding sections, we have shown that spatial axonal conduction is jointly regulated by the hyperpolarization-activated current (controlled by g_h), D, and the stimulation frequency set by T_s. To visualize the combined influence of these parameters, Fig. 4 presents contour maps of R in the (T_s, D) plane for three representative values of g_h: (a) $g_h = 0$ mS/cm^2, (b) $g_h = 1.27$ mS/cm^2, and (c) $g_h = 2.54$ mS/cm^2. In each panel, R ranges from 0 to 1 and is encoded using a 12-level color scale, where blue denotes complete conduction block ($R = 0$) and red corresponds to faithful conduction ($R = 1$). Intermediate colors represent partial conduction with $0 < R < 1$. The color bar is labeled at $R = 0$, 0.5, and 1, and the contour line corresponding to $R = 0.5$ is highlighted by a thin black curve. Across all three panels, regions of faithful conduction (red) are predominantly located in the upper-right portion of the (T_s, D) plane. Within a certain parameter range, increasing either T_s or D enhances R, indicating that lower stimulation frequencies and stronger spatial diffusion favor stable axonal propagation. Importantly, as g_h increases, the red region expands markedly from the upper-right corner toward smaller values of T_s and D. This expansion is particularly pronounced along the T_s direction, suggesting that enhanced I_h expression effectively counteracts the destabilizing effects of high-frequency stimulation. Meanwhile, increasing D further enlarges the faithful conduction region, indicating that stronger spatial diffusion can partially compensate for short stimulation periods. Together, these results demonstrate that I_h plays a critical role in enlarging the parameter space that supports reliable axonal conduction.

In addition to R, the CV provides an important quantitative measure of axonal signal conduction. Based on the contour map of R in the (T_s, D) plane for $g_h = 2.54$ mS/cm^2, faithful conduction is observed when both the stimulation period T_s and the diffusion coefficient D are sufficiently large. Therefore, CV is evaluated only within the parameter regions where $R = 1$, ensuring that action potentials propagate reliably along the axon. When the stimulation period is fixed at $T_s = 19$ ms, CV is calculated for diffusion coefficients in the range $D \in [0.0005, 0.0008]$ cm^2/ms. The resulting relationship between CV and D is shown in Fig. 5(a). CV increases monotonically with D, indicating that stronger spatial diffusion enhances the speed of action potential propagation along the axon.

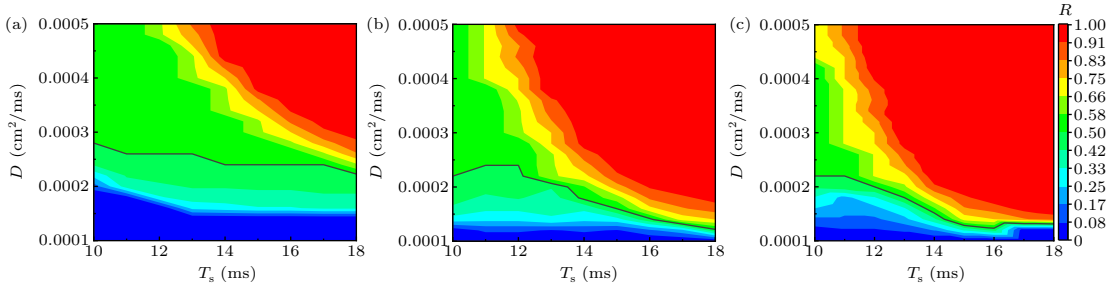


Fig. 4. Contour map of R in the (T_s, D) plane for different g_h. (a) $g_h = 0$ mS/cm^2, (b) $g_h = 1.27$ mS/cm^2, and (c) $g_h = 2.54$ mS/cm^2. The color map represents R ranging from 0 (blue, complete conduction failure) to 1 (red, fully faithful conduction without spike loss). Twelve uniformly spaced color levels are used, and the corresponding numerical values of R are explicitly labeled in panel (c) to provide a direct quantitative reference. Intermediate colors ($0 < R < 1$) indicate conduction failure manifested as spike loss during propagation. The thin black contour denotes the boundary $R = 0.5$, separating low- and high-reliability regimes.

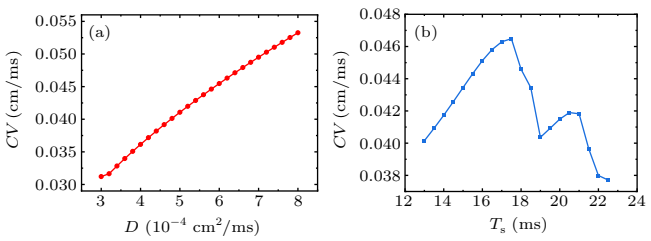


Fig. 5. *CV* of action potentials under faithful conduction conditions for $g_h = 2.54$ mS/cm^2. (a) *CV* as a function of the diffusion coefficient D with the stimulation period fixed at $T_s = 19$ ms, showing a monotonic increase of *CV* with increasing axial diffusion. (b) *CV* as a function of the stimulation period T_s at $D = 0.0005$ cm^2/ms, exhibiting oscillatory modulation with decreasing amplitude as T_s increases.

Conversely, when the diffusion coefficient is fixed at $D = 0.0005$ cm^2/ms, *CV* is computed for stimulation periods in the range $T_s \in [13, 22.5]$ ms, as shown in Fig. 5(b). In this case, *CV* exhibits a nonmonotonic dependence on T_s, with two local maxima and one local minimum. Although faithful conduction is maintained throughout this parameter range, the overall amplitude of *CV* decreases as T_s increases, reflecting the complex frequency-dependent modulation of axonal conduction dynamics.

To further quantify the influence of the hyperpolarization-activated conductance on propagation dynamics, we examined the dependence of conduction velocity (*CV*) on g_h at fixed $T_s = 20$ ms and $D = 0.0005$ cm^2/ms. As shown in Fig. 6(a), *CV* exhibits a nonmonotonic dependence on g_h. For small values of g_h ($0 \le g_h \le 1.22$ mS/cm^2), *CV* increases monotonically, reaching a maximum of 0.0439 cm/ms at $g_h = 1.22$ mS/cm^2. A further increase of g_h leads to a gradual reduction of *CV*, with a local minimum near $g_h = 1.76$ mS/cm^2, followed by a weak recovery at larger g_h, approaching a quasi-saturated regime.

This nonmonotonic behavior reflects the interplay between enhanced excitability induced by moderate g_h and the recovery dynamics of sodium channels. Moderate g_h elevates the resting membrane potential, bringing it closer to the excitation threshold and steepening the action potential upstroke, thereby increasing *CV*. In contrast, excessive g_h produces a sustained depolarizing bias that partially reduces sodium channel availability, weakening the depolarizing drive and slightly reducing the maximal upstroke rate.

Before analyzing bifurcations, it is important to clarify the role of spatial diffusion. In the HH cable model, diffusion represents axial current flow along the axon and determines whether local excitations can propagate to neighboring regions. While it influences conduction reliability, it does not fundamentally change the intrinsic bifurcation structure of the membrane model. Consequently, the single-compartment HH system provides a valid framework for studying how g_h affects excitability and recovery dynamics.

Figure 6(b) presents the bifurcation diagram of the membrane potential V as a function of g_h for the single-compartment HH model without diffusion. For small g_h, the system has a single stable resting state that gradually depolarizes as g_h increases. At $g_h = 3.69$ mS/cm^2, a saddle-node bifurcation produces a pair of limit cycles, creating a bistable regime. The nonmonotonic *CV* observed in Fig. 6(a) occurs entirely in the monostable regime, reflecting pre-bifurcation dynamical effects. These results indicate that *CV* is sensitive not only to diffusion and stimulus frequency, but also to intrinsic excitability changes governed by the bifurcation structure.

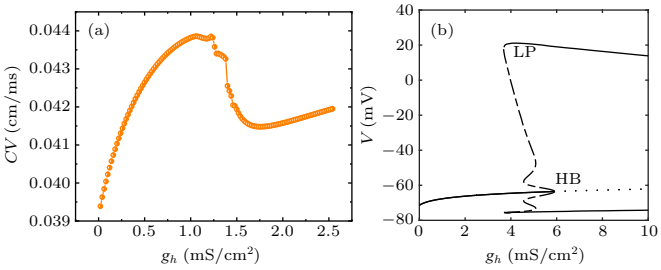


Fig. 6. Influence of hyperpolarization-activated conductance g_h on conduction velocity (*CV*) and membrane dynamics. (a) *CV* as a function of g_h at fixed $T_s = 20$ ms and $D = 0.0005$ cm^2/ms. *CV* increases for small g_h, reaches a local maximum near $g_h = 1.22$ mS/cm^2, and exhibits a shallow minimum near $g_h = 1.76$ mS/cm^2. (b) Single-parameter bifurcation diagram of membrane potential V as a function of g_h for the HH model without spatial diffusion. Thick solid lines indicate stable equilibrium points, and dotted lines indicate unstable equilibrium points. Maxima and minima of limit cycles are shown by thin solid (stable) and dashed (unstable) lines, respectively. The line conventions in all other bifurcation diagrams in this paper follow this scheme. Bi-stability emerges only for $g_h > 3.69$ mS/cm^2, beyond the range explored in panel (a).

3.2. Temperature effects on conduction and bifurcation mechanisms

To investigate how physiological temperature influences axonal signal conduction, temperature is introduced as a global control parameter in the HH cable model. Unlike intrinsic conductance modulation discussed previously, temperature primarily affects neuronal behavior by regulating ion-channel kinetics and membrane excitability. Experimental studies on hyperpolarization-activated cyclic nucleotide–gated (HCN) channels have shown pronounced temperature sensitivity in both activation rates and voltage dependence.[26]

In this work, temperature dependence is incorporated via a unified Q_{10}-based scaling framework, with the reference temperature set to $T_{\rm ref} = 25$ °C. Unless otherwise specified, simulations use $D = 0.0004$ cm^2/ms, $g_h = 2.54$ mS/cm^2, and $T_s = 20$ ms. Within this framework, temperature systematically modulates ion-channel kinetics, maximal conductances, and activation characteristics while preserving the structural form of the HH cable equations.

The kinetic rates of the sodium and potassium gating variables are scaled by a common temperature factor

$$\phi(T) = Q_{10,\rm gate}^{(T-T_{\rm ref})/10}, \tag{4}$$

where $Q_{10,\rm gate} = 3$ represents the experimentally determined temperature sensitivity of channel gating. The gating equations become

$$\frac{{\rm d}m}{{\rm d}t} = \phi(T)\,[\alpha_m(V)(1-m) - \beta_m(V)m],$$

$$\frac{\mathrm{d}h}{\mathrm{d}t} = \phi(T)\left[\alpha_h(V)(1-h) - \beta_h(V)h\right],$$
$$\frac{\mathrm{d}n}{\mathrm{d}t} = \phi(T)\left[\alpha_n(V)(1-n) - \beta_n(V)n\right]. \quad (5)$$

For the hyperpolarization-activated cation current I_h, temperature affects both the activation voltage and the time constant. The gating variable H follows:

$$\frac{\mathrm{d}H}{\mathrm{d}t} = \frac{H_\infty(V,T) - H}{\tau_H(V,T)}. \quad (6)$$

The steady-state activation includes a linear temperature-dependent voltage shift:

$$H_\infty(V,T) = \frac{1}{1+\exp\left(\frac{V-(-85+S(T-T_{\mathrm{ref}}))}{7.3}\right)}, \quad (7)$$

where $S = 0.87$ mV/°C is the temperature shift coefficient. The time constant is scaled as

$$\tau_H(V,T) = \frac{\tau_H(V)}{\phi_\tau(T)}, \quad \phi_\tau(T) = Q_{10,\tau}^{(T-T_{\mathrm{ref}})/10}, \quad (8)$$

with $Q_{10,\tau} = 2$. The temperature dependence of the maximal I_h conductance is incorporated via

$$g_h(T) = g_{h,\mathrm{ref}} \cdot Q_{10,g}^{(T-T_{\mathrm{ref}})/10}, \quad g_{h,\mathrm{ref}} = 2.54\ \mathrm{mS/cm^2},$$
$$Q_{10,g} = 1.436. \quad (9)$$

Under this formulation, temperature acts as a global control parameter that consistently modulates membrane excitability and ion-channel kinetics while preserving the structural integrity of the HH cable model.

Figure 7 summarizes the resulting spatiotemporal propagation patterns along the axon at different temperatures. At low temperature ($T = 10$ °C), only three action potentials are generated at the stimulation site within the 500–700 ms interval, all of which propagate successfully to the distal end ($R = 1$). However, this spike count is far below the ten expected from the stimulation period, indicating that cooling primarily suppresses spike generation rather than spatial propagation. A similar but weaker effect is observed at $T = 15$ °C, where five spikes are generated and transmitted without loss. At the reference temperature ($T = 25$ °C), ten action potentials are produced and propagate regularly, corresponding to stable and faithful conduction. In contrast, at elevated temperature ($T = 29$ °C), more than twenty action potentials are observed at the axonal terminal within the same time window, demonstrating accelerated spike generation and a restructuring of spike timing. These results indicate that temperature modulates axonal conduction both through changes in conduction reliability and through effects on spike generation and propagation speed. Notably, a conduction ratio $R = 1$ does not necessarily imply faithful signal transmission, as temperature-induced suppression or enhancement of spiking can substantially alter the effective information flow along the axon.

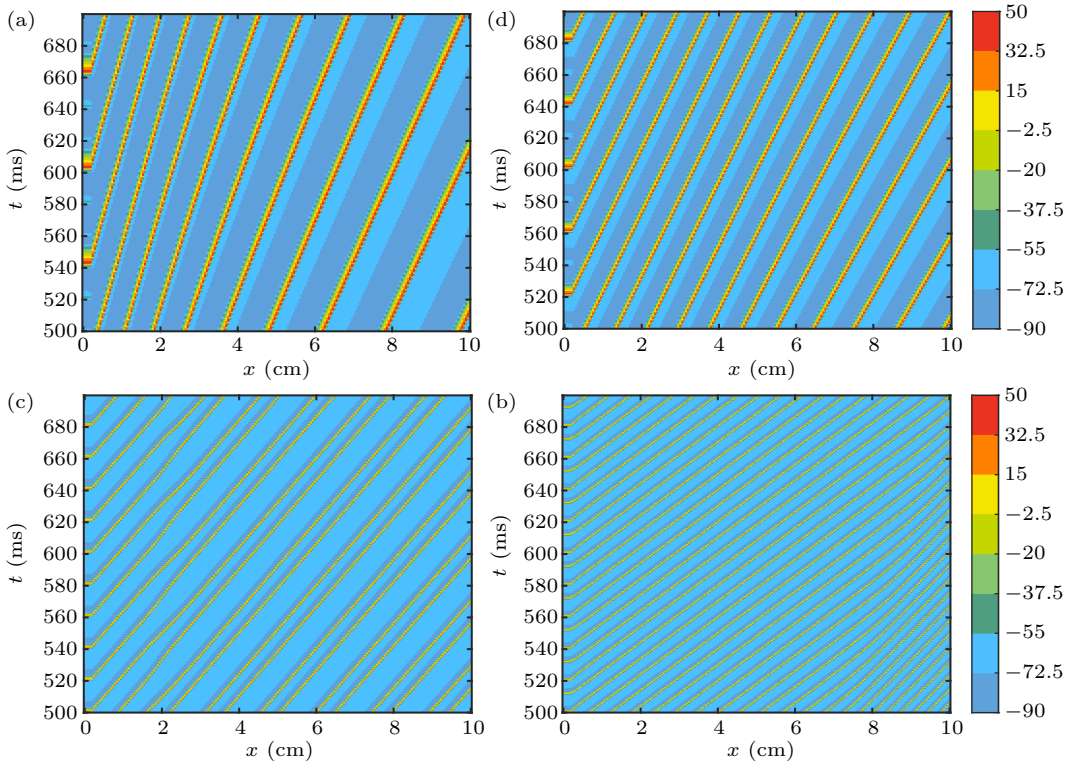


Fig. 7. Temperature-dependent spatiotemporal propagation of action potentials along the axon for $D = 0.0004$ cm^2/ms, $g_h = 2.54$ mS/cm^2, and $T_s = 20$ ms. Panels show membrane potential propagation at different temperatures: (a) $T = 10$ °C, (b) $T = 15$ °C, (c) $T = 25$ °C, and (d) $T = 29$ °C. Increasing temperature accelerates spike propagation and alters the conduction pattern, illustrating the strong temperature dependence of axonal dynamics.

To elucidate the underlying dynamical mechanisms, we next analyzed the bifurcation structure of the single-compartment HH model without spatial diffusion. Figure 8(a) shows membrane potential bifurcation diagrams as a function of the applied current I_{app} at two representative temperatures, $T = 25$ °C and $T = 27$ °C, with $g_h = 2.54$ mS/cm^2. Increasing temperature shifts the saddle-node (LP) and Hopf (HB) bifurcation points toward lower values of I_{app}, indicating an earlier entry into the bistable regime. This advance of bifurcation boundaries implies enhanced excitability and greater sensitivity to perturbations, consistent with the altered spike timing observed in the spatiotemporal simulations at elevated temperatures. Although the bifurcation diagram at $T = 29$ °C is not shown due to numerical limitations, the trend suggests a further advance of bifurcation points, in agreement with the observed spike multiplication.

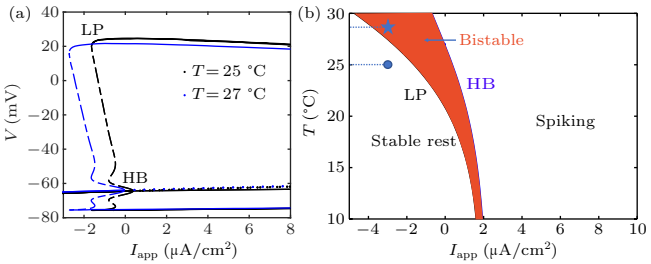


Fig. 8. Bifurcation analysis of the single-compartment HH model without diffusion for $g_h = 2.54$ mS/cm^2. (a) Membrane potential bifurcation diagram as a function of applied current I_{app} at $T = 25$ °C (black) and $T = 27$ °C (blue). Increasing temperature shifts the saddle-node (LP) and Hopf (HB) bifurcations to lower I_{app}, indicating enhanced excitability. (b) Two-parameter bifurcation diagram in the (I_{app}, T) plane, showing LP and HB curves that partition the parameter space into resting, bistable, and repetitive firing regimes. Blue solid circle and pentagram mark the operating points used in axonal propagation simulations at $T = 25$ °C and $T = 29$ °C, respectively; the latter lies within the bistable region. The bistable regime provides a dynamical explanation for the complex spike patterns observed at elevated temperatures.

The temperature-driven modulation of excitability is further illustrated in the two-parameter bifurcation diagram in the (I_{app}, T) plane, shown in Fig. 8(b), where the LP and HB curves partition the parameter space into resting, bistable, and repetitive firing regimes. The operating points corresponding to $T = 25$ °C and $T = 29$ °C are indicated. For the stimulation current used in the propagation study ($I_{\mathrm{app}} = -3$ μA/cm^2), lowering the temperature shifts the system deeper into the stable resting region, suppressing spike initiation (10–15 °C), whereas increasing temperature drives the system toward or into the bistable regime, explaining the spike multiplication observed at 29 °C. These results indicate that temperature modulates axonal signal conduction primarily by reshaping the intrinsic bifurcation structure of the membrane, rather than by altering spatial diffusion alone.

4. Conclusion

In this work, we systematically investigated axonal conduction failure using a HH cable model incorporating the hyperpolarization-activated current (I_h). Spatially resolved simulations reveal that conduction failure, manifested as spike loss during propagation, arises from the interplay of axial diffusion, stimulation timing, and intrinsic membrane dynamics, even when action potentials are reliably initiated near the stimulation site. Increasing the HCN conductance g_h substantially enlarges the parameter region supporting reliable conduction and reduces spike loss, as quantified by the conduction rate over the (T_{s}, D) plane.

Conduction velocity exhibits distinct dependencies on model parameters: it increases monotonically with diffusion strength but displays nontrivial, non-monotonic variations with both stimulation period and g_h, reflecting the complex interaction between wave propagation and membrane excitability. Moderate g_h enhances propagation reliability by depolarizing the resting membrane potential and expanding the stable conduction regime, whereas excessively large g_h diminishes propagation efficiency. Beyond an optimal conductance range ($g_h \gtrsim 1.2$ mS/cm^2), conduction velocity decreases and spike timing becomes distorted, highlighting the dual regulatory role of I_h in axonal signaling.

Temperature further modulates axonal propagation by altering excitability rather than diffusion. Cooling suppresses spike initiation, while heating promotes spike clustering and multiplication. Bifurcation analysis attributes these effects to temperature-dependent shifts of saddle-node and Hopf bifurcation boundaries, driving the system toward bistable and repetitive firing regimes. These results demonstrate that conduction failure is a dynamical consequence of parameter-dependent wave propagation in excitable media, and that HH cable modeling is essential for understanding both the reliability and speed of long-range axonal signaling.

Although our study focuses on type-II excitability described by the HH framework, the identified mechanisms are expected to generalize beyond this excitability class. In type-I excitable systems, where spike initiation occurs via a saddle-node on an invariant circle (SNIC) bifurcation, distinct propagation thresholds and recovery dynamics may emerge, potentially leading to different forms of conduction instability. Investigating spatial propagation reliability across excitability types represents an important direction for future research. Furthermore, while the present study considers deterministic dynamics to isolate intrinsic mechanisms, stochastic perturbations from channel noise or synaptic fluctuations may influence propagation reliability, particularly near bifurcation boundaries. Incorporating stochastic effects into cable axonal models may therefore provide a more realistic description of neural signal conduction and constitutes a promising avenue for future investigation.

Acknowledgment

Project supported by the National Natural Science Foundation of China (Grant No. 12172269).

References

[1] Weidner C, Schmelz M, Schmidt R, Hammarberg B, Østavik K, Hilliges M, Torebjörk H E and Handwerker H O 2002 *J. Neurosci.* **22** 6704
[2] Debanne D 2004 *Nat. Rev. Neurosci.* **5** 304
[3] Debanne D and Boudkkazi S 2010 *New Aspects of Axonal Structure and Function* (Boston : Springer US) pp. 55
[4] Swadlow H A, Kocsis J D and Waxman S G 1980 *Annu. Rev. Biophys.* **9** 143
[5] Swadlow H A and Waxman S G 1976 *Exp. Neurol.* **53** 128
[6] Bullock T H 1951 *J. Physiol.* **114** 89
[7] Hodgkin A L and Huxley A F 1952 *J. Physiol.* **117** 500
[8] Bielefeldt K and Jackson M B 1993 *J. Neurophysiol.* **70** 284
[9] Soleng A F, Chiu K and Raastad M 2003 *J. Physiol.* **552** 459
[10] Bean B P 2007 *Nat. Rev. Neurosci.* **8** 451
[11] Ratté S, Hong S, De Schutter E and Prescott S A 2013 *Neuron* **78** 758
[12] Tigerholm J, Petersson M E, Obreja O, Eberhardt E, Namer B, Weidner C, Lampert A, Carr R W, Schmelz M and Fransén E 2015 *Biophys. J.* **108** 1057
[13] Rama S, Zbili M and Debanne D 2018 *Curr. Opin. Neurobiol.* **51** 37
[14] Yan H, Yan J, Yu L and Shao Y F 2024 *Chin. Phys. B* **33** 058801
[15] Sun J, Li X, Sun Y, Xiong Z and He J 2026 *Chin. Phys. B* **35** 010501
[16] Pape H C and McCormick D A 1989 *Nature* **340** 715
[17] Tang Z Q and Trussell L O 2015 *J. Neurosci.* **35** 4540
[18] Biel M, Wahl-Schott C, Michalakis S and Zong X 2009 *Physiol. Rev.* **89** 847
[19] Khurana S, Remme M W H, Rinzel J and Golding N L 2011 *J. Neurosci.* **31** 8936
[20] Orio P, Parra A, Madrid R, González O, Belmonte C and Viana F 2012 *J. Neurophysiol.* **108** 3009
[21] Byczkowicz N, Eshra A, Montanaro J, Trevisiol A, Hirrlinger J, Kole M H, Shigemoto R and Hallermann S 2019 *eLife* **8** e42766
[22] Lu M, Gu H and Zhang X 2024 *Cogn. Neurodyn.* **18** 2433
[23] Tigerholm J, Petersson M E, Obreja O, Lampert A, Carr R, Schmelz M and Fransén E 2014 *J. Neurophysiol.* **111** 1721
[24] Hodgkin A L 1954 *J. Physiol.* **125** 221
[25] Ermentrout B 2002 *Simulating, Analyzing, and Animating Dynamical Systems: A Guide to XPPAUT for Researchers and Students* (Philadelphia: SIAM)
[26] Wu Y, Wang Q, Granger J, Reyes Gaido O, Lopez-Cecetaite G, Aguilar E N, Ludwig A, Moroni A, Bianchet M A and Anderson M E 2025 *Nat. Commun.* **16** 2102